Journal of Controlled Release 323 (2020) 463–474

Contents lists available at ScienceDirect

Journal of Controlled Release

journal homepage: www.elsevier.com/locate/jconrel

ApoE mimetic peptide targeted nanoparticles carrying a BRD4 inhibitor for treating Medulloblastoma in mice

Qiyue Wang[a], Virender Kumar[a], Feng Lin[a], Bharti Sethi[a], Donald W. Coulter[b], Timothy R. McGuire[c], Ram I. Mahato[a,*]

[a] Department of Pharmaceutical Sciences, University of Nebraska Medical Center, Omaha, NE 68198, USA
[b] Department of Pediatrics, University of Nebraska Medical Center, Omaha, NE 68198, USA
[c] Department of Pharmacy Practice, University of Nebraska Medical Center, Omaha, NE 68198, USA

ARTICLE INFO

Keywords:
Medulloblastoma
ApoE mimetic peptide
JQ1
BRD4
Nanoparticles
Biodistribution

ABSTRACT

Treatment of medulloblastoma (MB) is challenging due to diverse genetic make-up, chemoresistance and inefficient drug transport across the blood brain barrier (BBB). Since hedgehog (Hh) signaling regulates cancer cell proliferation and tumorigenicity, Hh inhibitors have the potential to treat sonic Hh driven MB (SHH-MB), but their repeated use develops chemoresistance due to mutations in smoothened (SMO). Herein, we aimed to overcome these problems by modulating GLI transcription using JQ1, which is a small molecule BRD4 inhibitor. JQ1 inhibited HD-MB03 and DAOY cell proliferation, with the IC_{50} of 402 and 4220 nM, respectively. JQ1 inhibited colony formation, but increased apoptosis in HD-MB03 and DAOY cells. Western blot analysis confirmed significant inhibition of GLI1 and c-MYC protein expression in DAOY and HD-MB03 cells, respectively. JQ1 was encapsulated into apolipoprotein (ApoE) mimetic peptide decorated nanoparticles (ApoE-NPs), with the mean particle size of 64 nm and drug loading of 10% (*w*/w). ApoE-NPs increased JQ1 concentration in the tumor by 5 and 8 folds at 6 and 24 h after systemic administration into orthotopic MB tumor bearing NSG mice compared to non-targeted JQ1 loaded NPs. Although there was also modest increase in JQ1 delivery to the liver, there was no hepatotoxicity as evidenced by H&E staining and little increase in serum ALT and AST after treatment with JQ1 loaded ApoE-NPs. There was also significant decrease in the orthotopic MB tumor burden after systemic administration of JQ1 loaded ApoE- NPs at the dose of 10 mg/kg every 3rd day for a total of 8 injections. In conclusion, JQ1 loaded NPs have the potential to treat Group 3 and SHH driven MB in mice.

1. Introduction

Medulloblastoma (MB) is an aggressively growing brain tumor in children. It spreads through cerebrospinal fluid (CSF) and metastasizes to different locations along the brain surface of the brain and spinal cord [1]. The 5-year survival rate for children with average-risk is 70–80%, whereas high-risk accounts for 60–65% [2]. The standard treatment of MB is the intensive adjuvant chemotherapy combined with high dose irradiation of the brain and spinal cord, but this treatment protocol has only 60% cure rate, and usually results in growth impairment, endocrine disorders, and neurocognitive deficits [3,4]. Therefore, more effective, less toxic therapeutics are urgently needed for MB, which is classified into four different subgroups, each with different origins, pathogenesis, and potential therapy targets [5]. SHH-MB subgroup represents ~30% of MB cases with an intermediate prognosis, mutations in PTCH and SMO proteins, and amplification of *GLI1/2* gene. Group 3 MB is one of the most aggressive subgroups account for approximately 25% of all MB with high metastatic potential and poor prognosis [5].

Bromodomain and extra-terminal domain (BET) family proteins, such as BRD2, BRD3, and BRD4 are related with recruited transcriptional activators [6]. BRD4 promotes progression and regulation of cell growth and transcription in neoplastic cell proliferation in different cancer types including neuroblastoma and glioblastoma [7,8]. Cerebellar granule neuron precursors (CGNPs) undergo rapid SHH-dependent expansion perinatally and excessive SHH pathway activity promotes MB. Most common *MYC* oncogenes include *c-MYC* and *MYCN*, which are at the crossroad of many biological pathways and processes involved in neoplastic cell growth and proliferation, which are frequently amplified in MB and are associated with a poor prognosis and

* Corresponding author at: Department of Pharmaceutical Sciences, University of Nebraska Medical Center (UNMC), 986025 Nebraska Medical Center, Omaha, NE 68198-6025, USA.
E-mail address: ram.mahato@unmc.edu (R.I. Mahato).

https://doi.org/10.1016/j.jconrel.2020.04.053
Received 20 March 2020; Received in revised form 22 April 2020; Accepted 30 April 2020
Available online 05 May 2020

tumor recurrence [4,9].

Since Hh signaling pathway regulates cell growth and cancer stem cell (CSC) proliferation, Hh inhibitors have the potential to treat SHH-MB [10]. Unfortunately, their repeated use develops chemoresistance because of mutations in SMO [11,12]. *N-MYC* is a downstream target of Hh whose induction can drive CGNP proliferation even in the absence of SHH signaling. Also, there is higher c-MYC expression in Group 3 MB. Herein, we treated SHH driven and Group 3 MB using JQ1, which is a small molecule BRD4 inhibitor [13,14]. SHH-MB can be treated by overcoming the problems created by SMO mutation because JQ1 can effectively modulate *GLI* transcription through BRD4 inhibition [6]. JQ1 can also be used to treat Group 3 MB by inhibiting *c-MYC* gene expression.

Since JQ1 is highly hydrophobic, it needs to be encapsulated into nanoparticles (NPs) for in vivo delivery to the tumor after systemic administration to minimize undesired toxicity. Additionally, nano-formulation ensures preferential accumulation of JQ1 in tumor cells via the enhanced permeability and retention (EPR) effect [15]. We previously reported methoxy poly(ethylene glycol)-*block*-poly(2-methyl-2-benzoxycarbonyl-propylene carbonate) (mPEG-PBC) conjugated polycarbonate-based polymer for drug delivery with high drug loading and low toxicity [16–18]. However, the blood-brain barrier (BBB) regulates drug transport to the brain. Successful treatment strategy of MB requires drugs to pass the BBB, which is a huge challenge for the disease treatment of central nervous system. Recently, use of noninvasive routes shows their utility for drug to delivery to the brain. The nanoplatform modified with antibodies or protein fragments could directly access into the brain via receptor-mediated endocytosis or transcytosis [19,20].

Apolipoprotein E (ApoE) is a chimera peptide composed of fats and proteins that binds to very low-density lipoprotein (VLDL) receptor for targeting NPs to the brain. However, ApoE molecular size is too big for accumulating therapeutic concentration in the brain. Therefore, we will decorate NP surface with ApoE mimetic peptide and facilitate JQ1 into brain with this ApoE mimetic peptide conjugated polymeric NPs. In this study, we determined the effect of JQ1 on orthotopic Group 3 MB bearing mice after systemic administration of ApoE mimetic peptide conjugated NPs carrying JQ1. Our previously reported PEG-PBC was synthesized and modified by ApoE-mimetic peptide COG133 to prepare JQ1 loaded NPs for brain targeting through low-density lipoprotein receptor (LDLR) mediated endocytosis.

2. Materials and methods

2.1. Materials

JQ1 was purchased from MedChem Express (Princeton, NJ). Dulbecco's Modified Eagle Medium (DMEM), Eagle's Minimum Essential Medium (EMEM), high glucose medium, Dulbecco's phosphate buffered saline (DPBS), and 0.25% trypsin were purchased from Hyclone (Logan, UT). Fetal bovine serum (FBS), antibiotic-antimycotic for cell culture, halt protease and phosphatase inhibitor cocktail (100×), Pierce BCA protein assay kit, and HEPES buffer were purchased from Millipore Sigma (St. Louis, MO). Human c-MYC primary antibody was purchased from Proteintech (Manchester, UK). Human GLI1 primary antibody, human MYCN primary antibody and GAPDH primary antibody was purchased from Santa Cruz Biotechnology (Dallas, TX). Human MB cell lines, such as DAOY and HD-MB03 cells were purchased from American Type Culture Collection (ATCC) (Manassas, VA), and were cultured in Eagle's Minimum Essential Medium (EMEM) and DMEM, respectively, containing 10% FBS and 1% penicillin/streptomycin in a humidified 37 °C incubator supplemented with 5% CO_2. Total RNA isolation kit was obtained from Qiagen (Gaithersburg, MD). TaqMan reverse transcription reagent kit was purchased from Life Technologies (Grand Island, NY). Radioimmunoprecipitation assay (RIPA) buffer and SYBR green-1 were purchased from (Roche, Indianapolis, IN). 3-(4,5-Dimethylthiazol-2-yl)-2,5-diphenyltetrazolium bromide (MTT) was purchased from Sigma Aldrich (St. Louis, MO). ApoE mimetic peptide (COG133) was purchased from Adooq Bioscience (Irvine, CA).

2.2. Cytotoxicity and colony formation assay

HD-MB03 and DAOY cells were cultured in 96-well plates at 5×10^3 per well in 100 μL DMEM and EMEM media under 5% CO_2 at 37 °C in a 95% humidified atmosphere, respectively. After 48 h post-treatment with various concentrations of JQ1, the cell viability was assessed by MTT (0.5 mg/mL) assay. Results are presented as the mean ± S.D. For clonony formation assay, HD-MB03 and DAOY cells were seeded at 250 cells/well into 6-well plates and allowed to attach for 24 h. Cells were then treated with JQ1 at the concentrations of 0, 2 and 4 μM for DAOY cells and 0, 400 and 800 nM for HD-MB03 cells. After a 7 day-incubation, colonies in each well were fixed by 10% formalin, stained with 0.5% crystal violet solution and visualized under a microscope. Then, the crystal violet was dissolved in 1.5 mL of 10% acetic acid solution and the optical density (OD) was measured at 590 nm. Each group was performed in triplicates.

2.3. Cycle and apoptosis analysis

HD-MB03 and DAOY cells pretreated with JQ1 concentrations of 0, 200 and 400 nM and 0, 2 and 4 μM, respectively for 48 h were harvested and fixed in 70% ethanol at 4 °C for 2 h. 1×10^6 cells were stained with 50 mg/mL propidium iodide (PI) for 30 min at room temperature in dark. Cell cycle distribution was analyzed by flow cytometry using BD Calibur flow cytometer (BD Biosciences, CA). For the apoptosis evaluation, 1×10^6 HD-MB03 and DAOY cells pretreated with JQ1 for 48 h were harvested and stained by Alexa Fluor 647-Annexin V and PI at room temperature for 30 min in dark. The apoptosis was analyzed by flow cytometry using a BD LSRII flow cytometer (BD Biosciences, CA).

2.4. C-MYC and GLI1 expression by real-time PCR and western blot analysis

To determine *c-MYC* and *GLI1* expression at mRNA and protein levels by real time RT-PCR and Western blot analysis after treating 3×10^5 HD-MB03 and DAOY cells per well in 6-well plates with 400 nM and 4 μM of JQ1 for 48 h, respectively. For real-time PCR analysis, treated HD-MB03 and DAOY cells were washed, lysed, and the total RNA was extracted using RNeasy mini kit. The concentration and purity of total RNA were determined by UV spectrophotometer at 260 and 280 nm. Multiscribe reverse transcription kit was employed to convert total RNA to cDNA per manufacturer's instruction (Applied Biosystems). SYBR Green-I dye universal PCR master was used to run RT-PCR on a LightCycler 480 Instrument (Roche) using primer as follows. Human *GLI1*: forward, 5′-CCA ACT CCA CAG GCA TAC AGG AT-3′; reverse, 5′-CAC AGA TTC AGG CTC ACG CTT C-3′. Human *c-MYC*: forward, 5′-CTG CGA CGA GGA GGA GAA CT −3′; reverse, 5′-GGC AGC AGC TCG AAT TTC TT-3′. Human *GAPDH* was used as a housekeeping gene: forward, 5′-ACC ACA GTC CAT GCC ATC AC -3′; reverse, 5′-TCC ACC ACC CTG TTG CTG TA-3′.

For Western blot analysis, total protein was isolated from HD-MB03 and DAOY cell lysates by incubating with RIPA lysis buffer and centrifuged by 10,000 ×*g* for 10 min at 4 °C. Protein concentration was determined using BCA™ protein assay kit (Thermo Scientific). Equal amounts of protein were separated in 4–15% mini PROTEAN polyacrylamide gel followed by transferring to polyvinylidene fluoride (PVDF) (Life Technologies, Carlsbad, CA) membranes by iBlot gel transfer system. Membranes were blocked with 1 × blocking buffer (LI-COR Biosciences, Lincoln, NE) for 2 h. Membranes were incubated with primary antibodies (1:1000 dilution) for c-MYC (10828–1-AP)

(Proteintech), GLI1 (sc-20,687), n-MYC (sc-53,993) and GAPDH (sc-365,062) (Santa Cruz Biotechnology, Inc.) for overnight. The next day, membranes were incubated with horseradish peroxidase-conjugated secondary antibodies (anti-mouse, sc-2055, anti-rabbit, sc-2054; and anti-goat, sc-2056; Santa Cruz Biotechnology, Dallas, TX). Specific protein bands were visualized by incubating the membrane with luminal reagent (sc-2048; Santa Cruz Biotechnology), and the images were recorded with FUJIFILM-LAS-4000 luminescent image analyzer (FUJIFILM Medical Systems Inc., USA). To ascertain comparative expression and equal loading of the protein samples, the membrane stained earlier was stripped and re-probed with GAPDH antibody.

2.5. Synthesis and characterization of ApoE mimetic peptide conjugated PEG-PBC polymer

Carboxyl poly(ethylene glycol)-*block*-poly(2-methyl-2-benzoxycarbonyl-propylene carbonate) (HOOC-PEG-PBC) was synthesized as described previously [21]. Briefly, 2, 2-bis(hydroxymethyl)propionic acid was stirred with benzyl bromide overnight to produce a white solid, benzyl 3-hydroxy-2-(hydroxymethyl)-2-methylpropanoate. Triphosgene was added to a round-bottom flask containing benzyl 2, 2-bis (methylol)propionate and reacted for 3 h, yielding another white solid, 2-methyl-2-benzyloxycarbonyl-propylene carbonate (MBC). HOOC-PEG-PBC was synthesized by 1, 8-diazabicyclo[5.4.0]undec-7-ene (DBU) catalyzed ring-opening polymerization between HOOC-PEG-OH and MBC. Finally, the amidation between HOOC-PEG-PBC (0.044 mmol, 600 mg) and COG133 (0.048 mmol, 100 mg) afforded COG133 conjugated polymer COG133-PEG-PBC in the presence of 1-ethyl-3-(3-dimethylaminopropyl)carbodiimide (EDC) (0.66 mmol, 126.7 mg), N-hydroxysuccinimide (NHS) (0.33 mmol, 37.9 mg) and trimethylamine (1.32 mmol, 132 mg). The chemical structure of COG133-PEG-PBC was characterized by Proton Nuclear Magnetic Resonance (^{1}H NMR) and gel permeation chromatography (GPC) for determining the molecular weight.

2.6. Preparation and characterization of ApoE peptide conjugated JQ1 loaded nanoparticles

JQ1 loaded COG133 conjugated NPs (ApoE-NPs) were prepared by mixing methoxy poly(ethylene glycol)-*block*-poly(2-methyl-2-carboxyl-propylenecarbonate)-*graft*-dodecanol (mPEG-b-PCD) and COG133-PEG-PBC at 70:30 *w*/w in acetone, followed by nanoprecipitation. Briefly, 3 mg COG133-PEG-PBC polymer, 7 mg mPEG-b-PCD and 1 mg of JQ1 were dissolved in 100 μL acetone followed by slowly injected into 1 mL of PBS under magnetic stirring (1300 rpm) for 10 min at room temperature. The solution was evaporated under reduced pressure to remove acetone and then filtered through 0.22 μm filter (Millipore) to obtain the formulation. Mean particle size and size distribution were measured by dynamic light scattering (DLS) using a Malvern Zetasizer (Worcestershire, United Kingdom). To determine the surface morphology and particle size of NPs by Atomic Force Microscopy (AFM), the samples were diluted in PBS, deposited on mica modified with 1-(3-aminopropyl)-silatrane (APS), rinsed with de-ionized (DI) water, and dried with argon. Images were collected with MultiMode Nanoscope IV system (Bruker Instruments, Santa Barbara, CA) in tapping mode at ambient conditions. Silicon probes RTESPA-300 (Bruker Nano Inc., CA) with a resonance frequency of ~300 kHz and a spring constant of ~40 N/m were used for imaging at scanning rate for about 2.0 Hz. Images were processed using FemtoScan software (Advanced Technologies Center, Moscow, Russia).

The encapsulation efficiency (EE) and drug loading (DL) was measured by HPLC after dissolving NPs using acetonitrile under the following conditions: mobile phase: Acetonitrile: water (80:20), C18 column (250 × 4.6 mm, 5 μm, Alltech, Deerfield, IL), flow rate 1 mL/min) and column temperature was 25 °C. Drug loading and encapsulation efficiency were calculated using the following formulas:

$$\text{EE (\%)} = \text{Amount of JQ1 encapsulated/Amount of JQ1 added} \times 100\% \quad (1)$$

$$\text{DL (\%)} = \text{Amount of JQ1 encapsulated/Amount of polymer} \times 100\% \quad (2)$$

To evaluate JQ1 in vitro release, formulations were prepared and transferred into a dialysis bag with cutoff 1000 Da followed by placed in pH 7.4 PBS solution. At regular time intervals, 1 mL release media was collected and replaced by equal volume of fresh media. JQ1 concentration in release media was measured by HPLC-PAD as described above.

2.7. Cellular uptake of targeted nanoparticles

To measure the cellular uptake of NPs, HD-MB03 and DAOY cells were seeded in the 6 well plate with density of 2×10^5 cells/well and allowed to attach overnight. Culture medium was replaced with FBS-free medium and coumarin 6 loaded ApoE-NPs or non-targeted NPs (1% loading) were added with concentration of 100 μg/mL and plates were keeping culture for 4 h. MB cells were then collected and analyzed using flow cytometry.

2.8. ApoE targeted drug delivery to brain tumor of orthotopic MB mouse model

All the procedures involving animals were approved by the Institutional Animal Care and Use Committee (IACUC) of the University of Nebraska Medical Center and meet all the federal guidelines concerning animal experimentation to ensure proper care and use of laboratory animals for research. HD-MB03 cells were transduced with GFP and luciferase encoded lentivirus, sorted for GFP expression to obtain a luciferase-expressing population (> 95%) and then expanded in DMEM medium.

Luciferase expressing HD-MB03 cells were collected, washed, and resuspended in PBS. A small hole, which situated 1 mm posterior of lambdoid suture of the scalp over the cerebellum and 1 mm lateral of sagittal suture, was drilled into the skull bone on anesthetized NSG mice (females, 6–8 week old). 1×10^5 cells were stereotactically injected 2 mm deep into cerebellum using Hamilton syringe.

For quantification of JQ1 concentration in the brain and other major organs, mice bearing orthotopic Group 3 MB were injected with JQ1 loaded ApoE mimetic peptide conjugated and non-targeted NPs. At 6 and 24 h post injection, blood was withdrawn via cardiac puncture before mice were euthanized and major organs including the brain were collected, weighed, and homogenized for extraction of JQ1 from the tissue samples. Drug concentrations in the plasma and tissues were measured using LC-MS/MS (4000 QTRAP, AB, Sciex Inc.). Briefly, 100 mg of tissue samples were homogenized in 5 times HPLC grade water and spiked with OTX015 as an internal standard (IS) [22]. Subsequently, 1.0 mL of acetonitrile was added, followed by vortexing and high-speed centrifugation. The supernatant was evaporated to dryness, and the residue were reconstituted with 100 μL of acetonitrile: water (60:40, *v/v*). LC-MS/MS data acquisition will be performed by using Analyst® software on a QTRAP 4000 mass spectrometer. The mass spectrometer will be operated in the positively selected reaction monitoring (SRM) for JQ1 (*m/z* 401.0) and internal standard (*m/z* 383.0).

2.9. Organ histology and liver injury markers

Tissues of major organs such as liver, lung, kidney, heart and spleen isolated and cut into pieces and were fixed in 10% paraformaldehyde solution overnight and then embedded in paraffin. Sections of 5-mm thickness were stained with hematoxylin and eosin (H&E) by using standard protocols. Sections were scanned at 40× with the iScan HT Slide Scanner (Ventana Medical Systems, Tucson, AZ), and

representative views of sections are shown. Liver injury markers such as alanine aminotransferase (ALT) and aspartate aminotransferase (AST) levels in the serum were measured using the ALT and AST assay kits (Universal Biologicals Ltd. UK).

2.10. Antitumor effect of ApoE targeted JQ1 loaded nanoparticles in orthotopic MB mice

Orthotopic MB tumor was generated in NSG mice using stably luciferase expressing HD-MB03 cells. When the bioluminescence reached 2×10^6 p/s/cm^2/sr, mice were divided into 3 groups ($n = 5$): i) control group, ii) non-targeted NPs loaded with JQ1, and iii) ApoE-NPs loaded with JQ1. Formulations were injected via tail vein at the dose of 10 mg/kg every third day for four weeks. Mice were imaged by IVIS imaging system to monitor tumor growth. At the end of studies, mice were sacrificed and main organs were removed, fixed with 4% formaldehyde solution and embedded in paraffin. Effectiveness of the proposed therapy was determined by measuring apoptosis and metastasis. The slices tissues were stained by hematoxylin and eosin (H&E). Brain tissues were further stained with c-MYC, Ki67 and caspase-3 on MB samples by immunohistochemistry.

2.11. Statistical analysis

Data were expressed as mean ± S.D. Differences between groups were analyzed by one-way analysis of variance (ANOVA) and Tukey multiple comparisons tests. $^{*}p < .05$ was considered significant, and $^{**}p < .01$, $^{***}p < .001$ were considered highly significant.

3. Results

3.1. Anticancer activity and inhibition of colony formation

Cytotoxicity of JQ1 on MB cell lines was determined in HD-MB03 and DAOY cells by incubating these cells at different drug concentrations. As shown in Fig. 1A, there was dose-dependent cell killing, with the IC_{50} values of 402 nM and 4.22 μM in HD-MB03 and DAOY cells, respectively. The inhibitory effect of JQ1 on tumorigenic potential in MB cells was determined by colony formation assay by incubating these cells at two different concentrations: 2 and 4 μM for DAOY cells, but only 400 and 800 nM for HD-MB03 cells. JQ1 greatly reduced colony formation in a dose dependent manner (Fig. 1B). As shown in Fig. 1C, JQ1 could significantly inhibit colony formation at 24 h post treatment in both DAOY and HD-MB03 cells, with higher effect in inhibiting colony formation in HD-MB03 cells compared to DAOY cells. These results suggest that JQ1 is more effective in Group 3 MB.

3.2. JQ1 downregulated c-MYC and GLI1 expression

To confirm whether JQ1 can be used to treat both Group 3 and SHH driven MB, we determined the effect on c-MYC and GLI1 expression at mRNA and protein levels after incubating HD-MB03 and DAOY cells with 400 nM and 4 μM of JQ1 for 48 h, respectively. As shown in Fig. 2A, there was significant decrease in *c-MYC* and *GLI1* mRNA expression compared to those of un-treated control cells. Similarly, the expression of c-MYC and GLI1 at protein level in both DAOY and HD-MB03 cells was inhibited upon treatment with JQ1 for 48 h determined by Western blot analysis. There was also significant inhibition of n-MYC, which is downstream signals of GLI1, expression at protein level in both these cell lines (Fig. 2B and S1).

3.3. Cell cycle arrest and apoptosis

Cell cycle arrest was determined by propidium iodide (PI) staining after incubating DAOY and HD-MB03 cells with JQ1 for 48 h. For DAOY cells, results showed that treatment with JQ1 at 4 μM increased cell arrest in G1 phase compared to control group (66.9% vs. 42.2%), whereas small number of cells were arrested in S-phase (16.2%) and G2 phase (16.8%). Treatment of HD-MB03 cells with JQ1 at 400 nM caused 69.9% cell arrest in G1 phase from 50.1% in the control group, whereas only 13.1% of these cells were arrested in S-phase, and 17.0%, respectively in G2 phase (Fig. 3A and B). Further, apoptotic cell percentage was determined using a flow cytometer after staining with Alexa Fluor 647-Annexin V and PI. For DAOY cells, apoptotic cell population was significantly increased when the cells were treated with JQ1 at 4 μM compared to the control group (25.5% vs. 8.5%, respectively). Further, the apoptotic cell population increased to 26.6% from 8.26%, respectively when HD-MB03 cells were treated with 400 nM JQ1 (Fig. 3A and B).

3.4. Copolymer synthesis, formulation and characterization of JQ1 loaded nanoparticles

COG133-PEG-b-PBC copolymer was synthesized as shown in

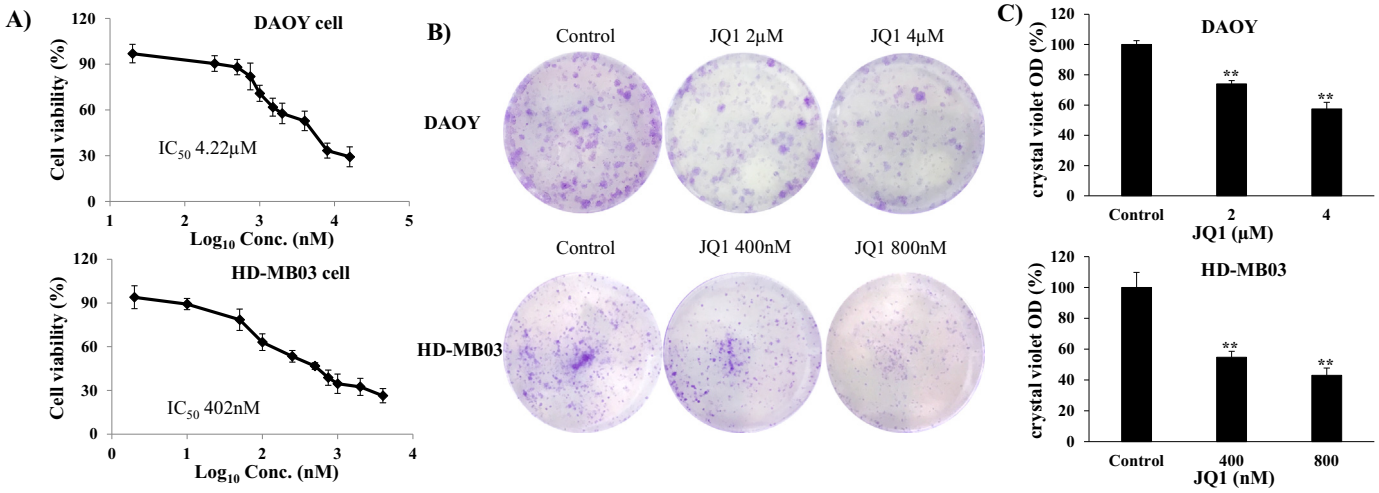

Fig. 1. A) Cytotoxic effect of JQ1 on HD-MB03 and DAOY cells. IC_{50} was calculated to be 402 nM and 4.22 μM in HD-MB03 and DAOY cells, respectively. B) Effect of JQ1 on colony formation in HD-MB03 and DAOY cell, while DAOY cells were treated at the doses of 0, 2 and 4 μM, we treated HD-MB03 cells with 0, 400 and 800 nM of JQ1 for 24 h. C) Effect of JQ1 on colony formation by quantified crystal violet. **, $p < .01$ (comparison between control vs JQ1 treated). (For interpretation of the references to colour in this figure legend, the reader is referred to the web version of this article.)

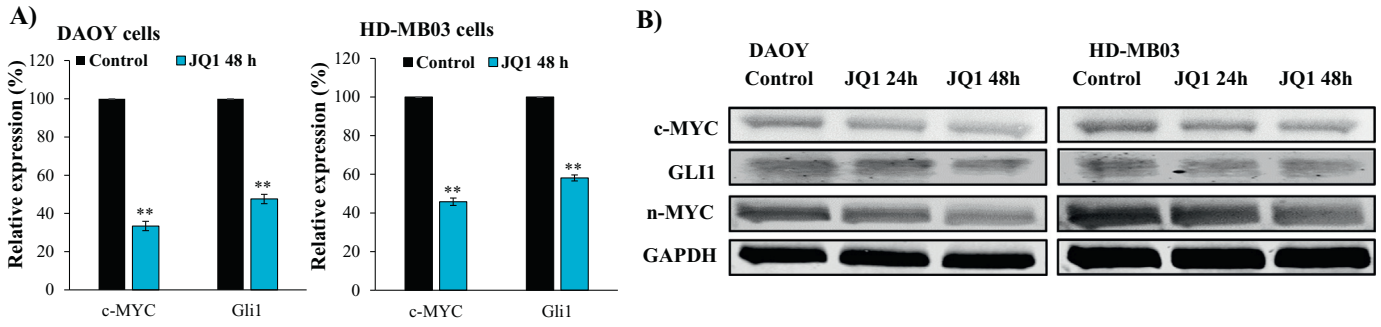

Fig. 2. Effect of JQ1 on c-MYC and GLI1 expression after treatment of DAOY and HD-MB03 cells for 48 h at the dose of 4 and 0.4 μM. A) Real time RT-PCR and B) Western blot analysis. **, $p < .01$ (comparison between control between JQ1 treated groups).

Fig. 4A. Briefly, 2-methyl-2-benzyloxycarbonyl-Propylene Carbonate (MBC) was produced by a two-step reaction: nucleophilic substitution of bromo group on benzyl bromide by carboxylic acid on 2, 2-bis(hydroxymethyl)propionic acid and subsequent cyclization by triphosgene. Afterwards, ring-opening polymerization yielded HOOC-PEG-PBC, which was then coupled by COG133 to afford COG133-PEG-b-PBC. The polymer was characterized by ^{1}H NMR (Fig. 4B). Based on the integration (456H) of the peak at 3.5 ppm for PEG, the degree of polymerization (DP) is 30, calculated from the integration of the peaks at 7.29 ppm (150H, $-C_6H_5$), 5.09 ppm (60H, $-CH_2$-Ar), 4.21 ppm (120H, $-OCH_{2-}$,) and 1.14 ppm (90H, $-CH_3$). The broad peak between 0.8 ppm and 3 ppm indicates the successful conjugation of COG133. Thus, the calculated molecular weight of this copolymer was 14,500 Da.

We prepared JQ1 loaded NPs owing to ease in synthesis, biocompatibility, and ability to form stable NPs. The mean particle size of JQ1 loaded NPs was 64.0 ± 0.46 nm with PDI of 0.230 as determined by DLS (Fig. 5A) and ζ potential of zero mV determined by Malvern Zetasizer. Surface morphology and particle size of these NPs were

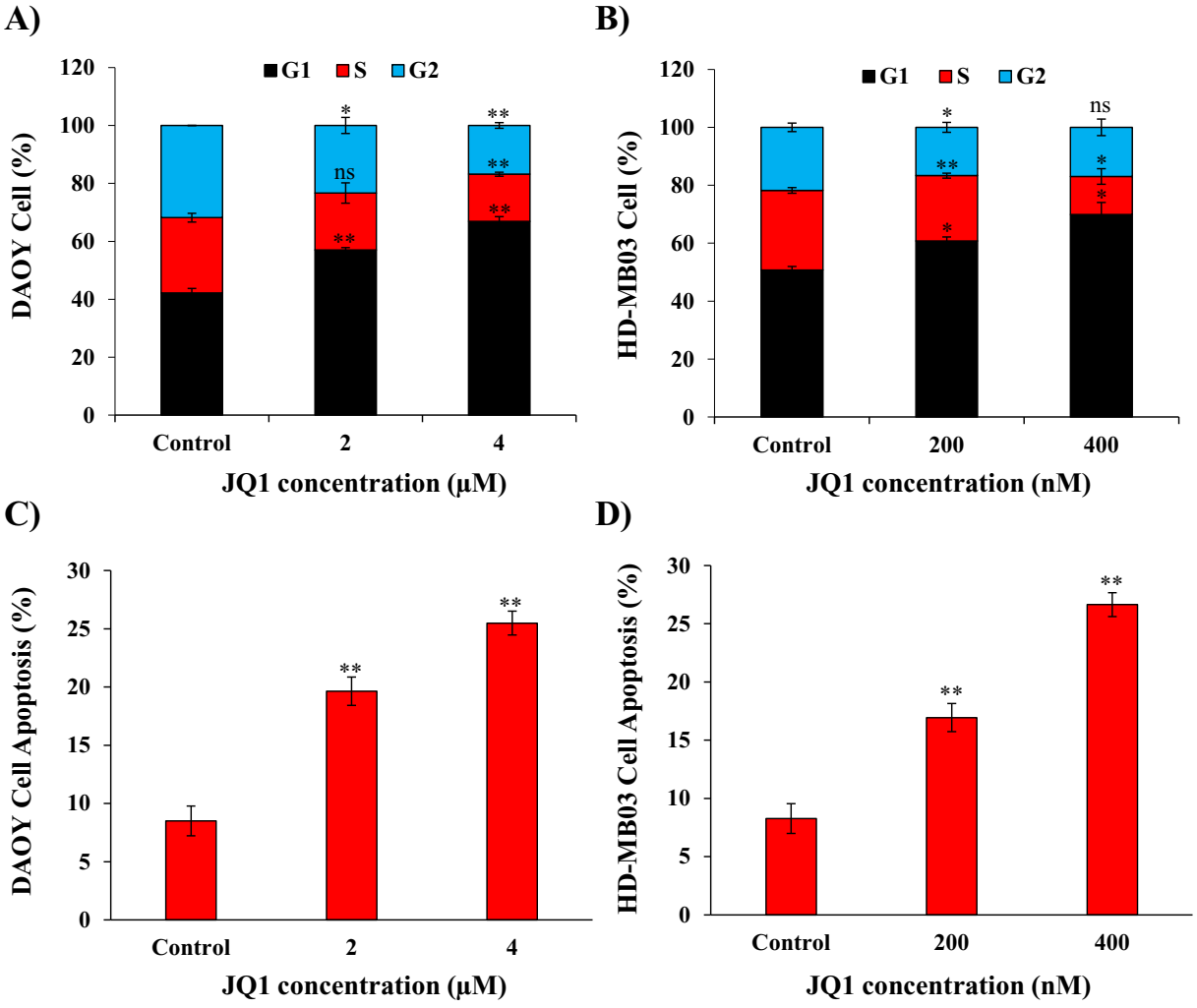

Fig. 3. Effect of JQ1 on cell cycle arrest and apoptosis in DAOY and HD-MB03 cells after incubation for 48 h. A) Cell cycle analysisand C) apoptosis of DAOY; B) Cell cycle analysis and D) apoptosis of HD-MB03 cells. *, $p < .05$ (comparison between control vs JQ1 treated), **, $p < .01$ (comparison between control vs JQ1 treated groups), ns, $p > .05$.

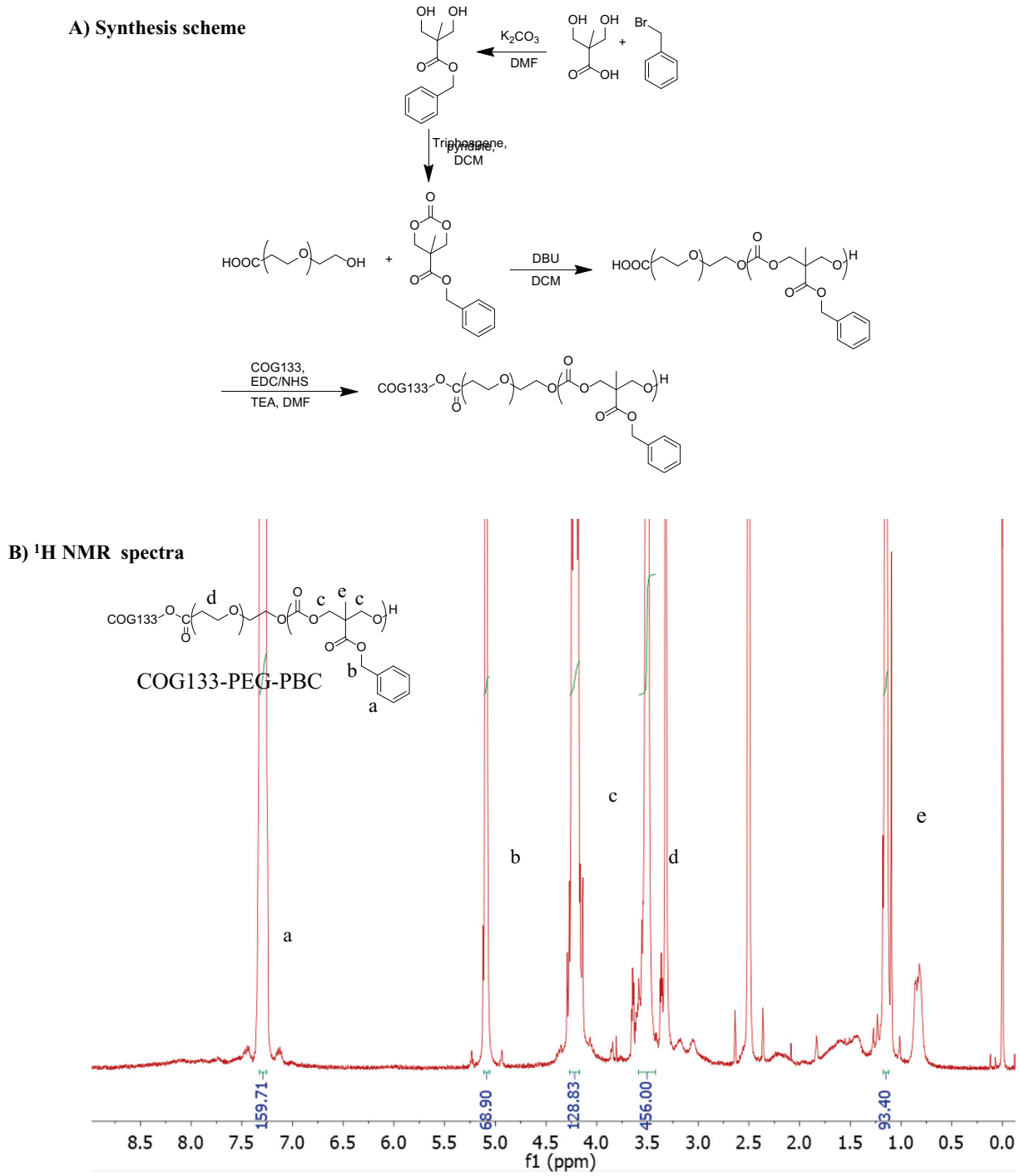

Fig. 4. Synthesis and characterization of ApoE mimetic peptide (COG-133) conjugated PEG-PBC polymer. A) Synthesis scheme and B) ^{1}H NMR spectra.

further determined by atomic force microscopy (AFM). These NPs were of spherical shape and had narrow particle size distribution, with the mean particle size of 62.52 nm (Fig. 5B and C). The drug loading determined by HPLC was 9.33% *w/w* at the theoretical loading of 10.0%. There was no batch to batch variation in particle size and drug loading. The release profile of JQ1 from NPs was determined by dialysis and results are shown in Fig. 5D. There was little effect of ApoE mimetic peptide conjugation on JQ1 release, with also almost 50% release in 48 h.

3.5. Cellular uptake of targeted nanoparticles

We prepared ApoE mimetic peptide (COG-133) conjugated and coumarin loaded NPs. ApoE mimetic peptide COG-133 has only 18 amino acids but retains LDL binding potential. The effect of these ApoE conjugation on the cellular uptake of NPs was determined after incubating HD-MB03 and DAOY cells with 100 μg/mL coumain 6 loaded (1% loading) ApoE-NPs or non-targeted NPs for 4 h. Both HD-MB03 and DAOY cells treated with coumarin 6 loaded ApoE-NPs displayed much higher uptake than those treated with non-targeted NPs (Fig. 6). Cellular uptake of ApoE-NPs was significantly reduced upon prior incubation with free COG-133 peptide (200 μg/mL) indicating that ApoE-

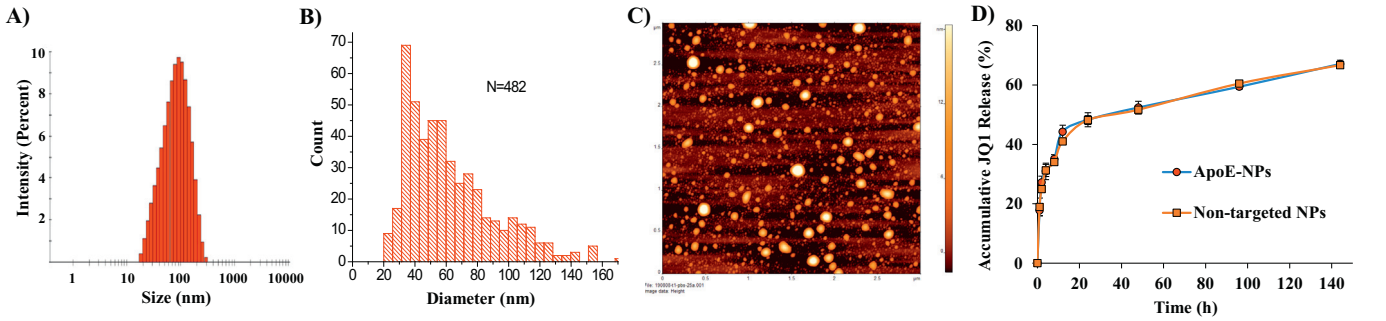

Fig. 5. Characterization of JQ1 loaded nanoparticles (NPs). A) Particle size distribution measured by dynamic light scattering (DLS), B) particle size distribution measured by atomic force microscopy (AFM), C) Surface morphology by AFM, and D) Release profiles of JQ1 from ApoE-NPs and non-targeted NPs.

NPs can be specifically taken up by MB cells via ligand-mediated endocytosis pathway (Fig. 6). In contrast to MB cells, these ApoE-NPs were poorly taken up by SVG p12 cell lines (Fig. S3).

3.6. ApoE targeted drug delivery of JQ1 to orthotopic MB tumor

Biodistribution of JQ1 was determined at 6 and 24 h post systemic administration of JQ1 loaded ApoE-NPs or non-targeted NPs at the dose of 10 mg/kg in orthotopic MB bearing NSG mice. Compared to non-targeted NP formulation, ApoE-NPs significantly increased JQ1 concentration in MB tumor in the brain at 6 h and 24 h post systemic administration into orthotopic Group3 MB bearing mice (Fig. 7). JQ1 loaded non-targeted NPs exhibited very low concentrations of 0.069 ± 0.014 ng/mg and 0.006 ± 0.002 ng/mg, respectively in the brain tumor sites, while ApoE-NPs showed an enhanced JQ1 concentration at the tumor site (0.311 ± 0.036 ng/mg and 0.060 ± 0.009 ng/mg (n = 4), respectively) at 6 h and 24 h post administration. The percentage of injected dose of JQ1 in the brain delivered by ApoE-NPs significantly increased compared to non-targeted NPs at both 6 h (0.051 ± 0.011% vs 0.016 ± 0.002%) and 24 h (0.014 ± 0.002% vs 0.001 ± 0.0005%). Although the mice receiving ApoE-NP formulation also showed modest increase in JQ1 concentration in the liver, but did not show statistics difference in JQ1 accumulation in heart, kidneys, lungs and spleen (Fig. 7).

3.7. Organ toxicity and liver injury markers

Systemic administration of JQ1 loaded ApoE-NPs and non-targeted NPs in orthotopic MB bearing NSG mice did not result hepatotoxicity as evidenced by H&E staining of the liver sections (Fig. 8A). We also measured liver injury markers like ALT and AST levels in the serum. There was no significant increase in ALT and AST levels compared to the sham operated control mice (Fig. 8B). Apart from no hepatotoxicity, these formulations were also safe to other major organs as well (Fig. S4). These results indicate that there was no drug induced liver injury occurs even after multi-injections when injected at the dose of 10 mg/kg.

3.8. Antitumor effect of JQ1 on orthotopic MB mouse models

After generating orthotopic MB tumors in NSG mice using stably luciferase expressing HD-MB03 cells, mice were injected intravenously with ApoE targeted and non-targeted NPs loaded with JQ1 at the dose of 10 mg/kg every 3 day for 4 weeks. Mice were imaged by IVIS to monitor tumor growth. As shown in Fig. 9A and B, mice treated with JQ1 loaded ApoE-NPs exhibited significant inhibition in tumor growth as evidenced by decrease in bioluminescence signals compared to the mice treated with JQ1 loaded non-targeted NPs and non-treated mice. We observed that body weights (Fig. 9C) and physical activities of mice were normal in both the treatment groups, whereas the control animals did not even survive during all treatment.

Brain tissue sections from different treatment groups were examined by H&E and immunohistochemistry (IHC) staining. H & E images confirmed the contained dense of MB cells in the control group. Furthermore, c-MYC was used for confirming the existence of MB mass as its remarkable high expression in Group 3 MB cells and could promote the cell cycle. Compared to the control and non-targeted NP group, the brain treated by JQ1 loaded ApoE-NPs significantly decrease the density of MB cells (Fig. 10A and B) which exhibited stronger antitumor efficiency. There was significant decrease in the number of cell proliferation marker Ki-67 positive cells but significant increase in apoptotic cell marker caspase 3 positive cells in the brain after treatment with JQ1 loaded ApoE-NPs compared to control and non-targeted NPs groups (Fig. 10C and D). To quantify positive cells, each section was scanned, and the number of positive cells out of total cells was quantified to calculate the ratio of positive cells. As shown in Fig. 10E to

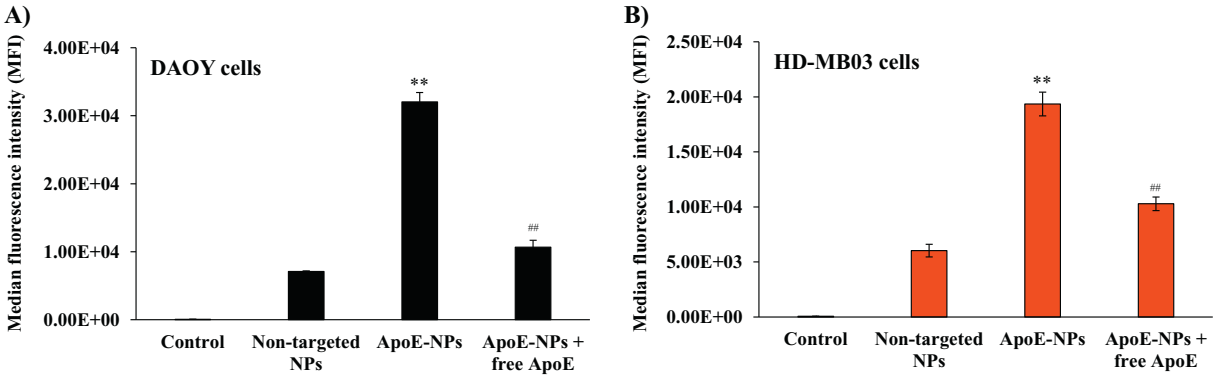

Fig. 6. Cellular uptake of ApoE mimetic conjugated nanoparticles (NPs) at 4 h post treatment. Pre-treatment of cells with free ApoE could reduce the cellular uptake. **, $p < .01$ (comparison between Non-targeted NPs vs ApoE-NPs), **, $p < .01$ (comparison between ApoE-NPs vs ApoE-NPs with free ApoE).

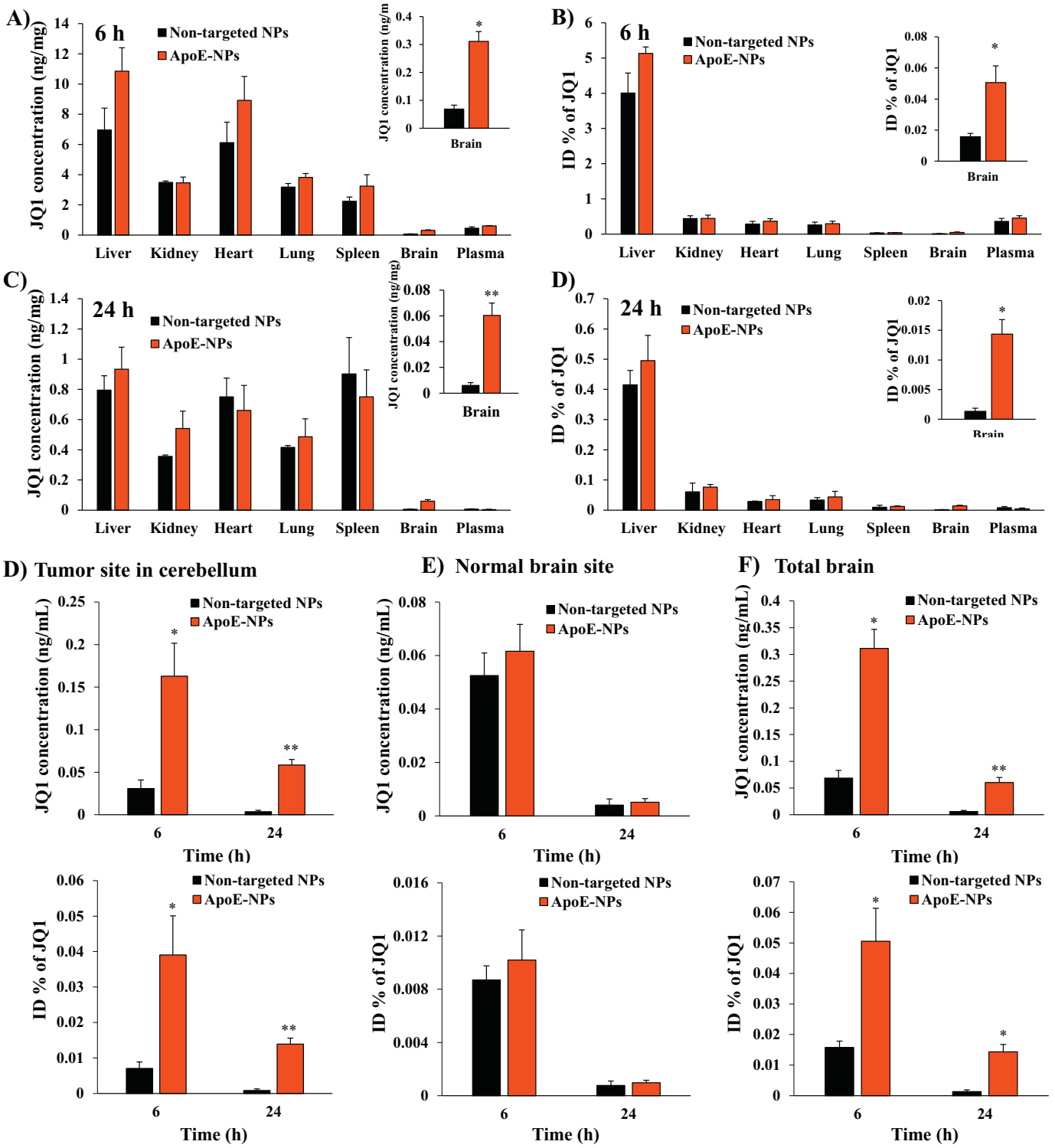

Fig. 7. Biodistribution of JQ1 at 6 and 24 h after systemic administration of JQ1 loaded ApoE mimetic peptide conjugated nanoparticles (ApoE-NPs) and non-targeted NPs in orthotopic MB bearing NSG mice at a dose of 10 mg/kg. A) JQ1 concentration at 6 h injection; B) % of injected dose (ID) of JQ1 at 6 h injection; C) JQ1 concentration at 24 h post injection; and D) % of injected dose at 24 post injection. JQ1 concentration and % of injected dose (ID) of JQ1 in D) Tumor site in cerebellum, E) normal brain and F) Total brain. Results are presented as the mean ± S.D. of three mice. *, $p < .05$; **, $p < .01$ (comparison between Non-targeted NPs vs ApoE-NPs).

G, the ratio of c-MYC and Ki-67 positive cells were significantly decreased, while more caspase 3 positive cells after treatment with JQ1 loaded ApoE-NPs compared to the control and non-targeted NP groups.

4. Discussion

Standard treatment strategies of brain tumors include surgery, radiation and chemotherapy [3,23,24]. While considering the surgically challenging anatomic location of MB, the surgery is not the best option.

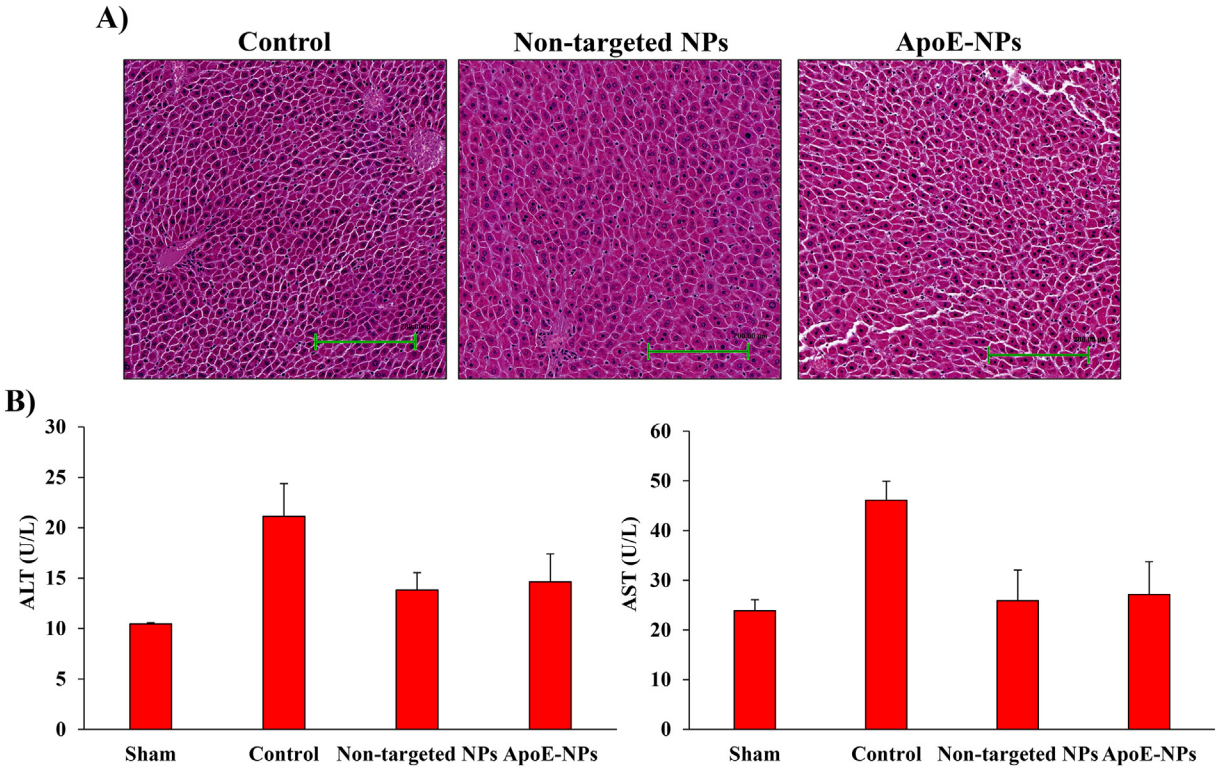

Fig. 8. Hepatotoxicity after systemic administration of ApoE-targeted and non-targeted nanoparticles (NPs) loaded with JQ1 into NSG mice at the dose of 10 mg/kg. After the third injection, blood was withdrawn by cardiac puncture and livers were isolated for Hematoxylin and eosin (H & E) staining. A) H & E staining of liver. B) Alanine transaminase (ALT) and aspartate transaminase (AST) levels in serum.

At the same time, radiation and chemotherapy could also cause obvious side effects including neurological deficits, endocrine disorders, and secondary cancers, which leaves very limited options for MB therapy. MB is a genetically heterogeneous disease. With the deep recognition of molecular pathogenesis and gene expression, different MB subgroups show variation in the activation of oncogenes which further complicate their treatment [25].

Multiple studies suggest that JQ1 could inhibit cancer cell proliferation through its effect on BRD4 binding to acetylated histones and inhibition of growth promoting transcription factor MYC [26]. *MYC* oncogene is at the crossroads of many biological pathways and processes involved in neoplastic cell growth and proliferation. Both SHH-MB and Group 3 MB related to MYC expression. *MYCN*, which is directly regulated by *GLI*, is a downstream target of SHH-MB while chromatin immunoprecipitation studies reveal BRD4 directly occupies *GLI* promoter site and increase its expression [6,27]. Furthermore, BRD4 could directly binding with promoter site of *c-MYC* gene and induce c-MYC expression which significantly amplified in Group 3 MB [26,28,29]. After treatment with JQ1 for 48 h, both DAOY cells (SHH-MB) and HD-MB03 cells (Group 3 MB) exhibited significant decrease in MYC protein expression (Fig. 2). The difference in cytotoxic effect of JQ1 between these two cell types (Fig. 1) was possibly caused by different levels of MYC expression by these two cell types (Fig. 2B), especially since c-MYC controls downstream targets such as cyclin A and cyclin E to reduce cell proliferation while n-MYC affects cell proliferation though cyclin D [25,30–32]. After treatment with JQ1, both DAOY and HD-MB03 cells were arrested on G1 phase and induce to apoptosis with a dose-depended effects.

Polymeric NPs are widely used for drug delivery to prolong the circulation and enhance drug accumulation to the tumor via passive targeting. BBB plays effectively role to protect the brain from circulating pathogens which also prevent drug's permeation into and produce treatment effects [33]. To bind with the receptors, polymeric carriers should be conjugated to endogenous receptor ligand, an antibody targeting the receptor or a mimetic peptide ligand. As transferrin receptor, insulin receptor, and low-density lipoprotein receptor (LDLR) are expressed on brain endothelial cells, conjugation of specific ligand to the polymer could increase drug delivery to the brain [34–36]. LDLR is a cell surface receptor, which mediates the endocytosis of cholesterol-rich LDL such as cholesterol, tocopherol, and apolipoproteins. Apolipoproteins have been conjugated to many nanomaterials to increase the brain transport [37,38]. COG-133 was ApoE mimetic peptide which could be recognized and binds to LDLR to increase the receptor-mediated endocytosis. Therefore, we modified PEG-PBC polymer by COG-133 and prepared polymeric NPs to encapsulate JQ1 by nanoprecipitation with particle size of 60 nm and drug loading of 9.3%. The hydrophilic PEG shell could avoid the uptake of NPs by the reticuloendothelial system (RES) and prolonged the circulation in bloodstream. There was no burst release of JQ1 was observed and approximately 65% of the drug was released in 144 h which confirmed ApoE-NPs could extend release period of drug loaded in the hydrophobic core (Fig. 5D).

The cellular uptake of ApoE-NPs was investigated. Both DAOY and HD-MB03 cells showed much higher uptake of ApoE-NPs compared to non-targeted NPs, indicating LDLR-mediated uptake by MB cell lines (Fig. 6). To confirm ApoE-NPs has the brain targeting ability, biodistribution of JQ1 loaded NPs was determined using LC-MS/MS to quantify JQ1 accumulation in major organs in Group 3 MB bearing mice. ApoE-NPs efficiently delivered JQ1 to the MB tumor in the brain (Fig. 7) by 5 and 8-folds higher at 6 h and 24 h after injection, compared to non-targeted NPs, suggesting efficient and specific drug delivery to MB tumor in the brain. However, there was little difference in JQ1 concentrations in the normal brain tissues of the MB tumor bearing mice treated with ApoE-NPs and non-targeted NP formulations. After co-incubation of targeted NPs with free ApoE mimetic peptide, the cellular uptake of NPs was significantly decreased, which indicating ApoE-NPs was taken up by MB cells via LDL receptor mediated endocytosis pathway. Although there are reports that COG-133 hard to

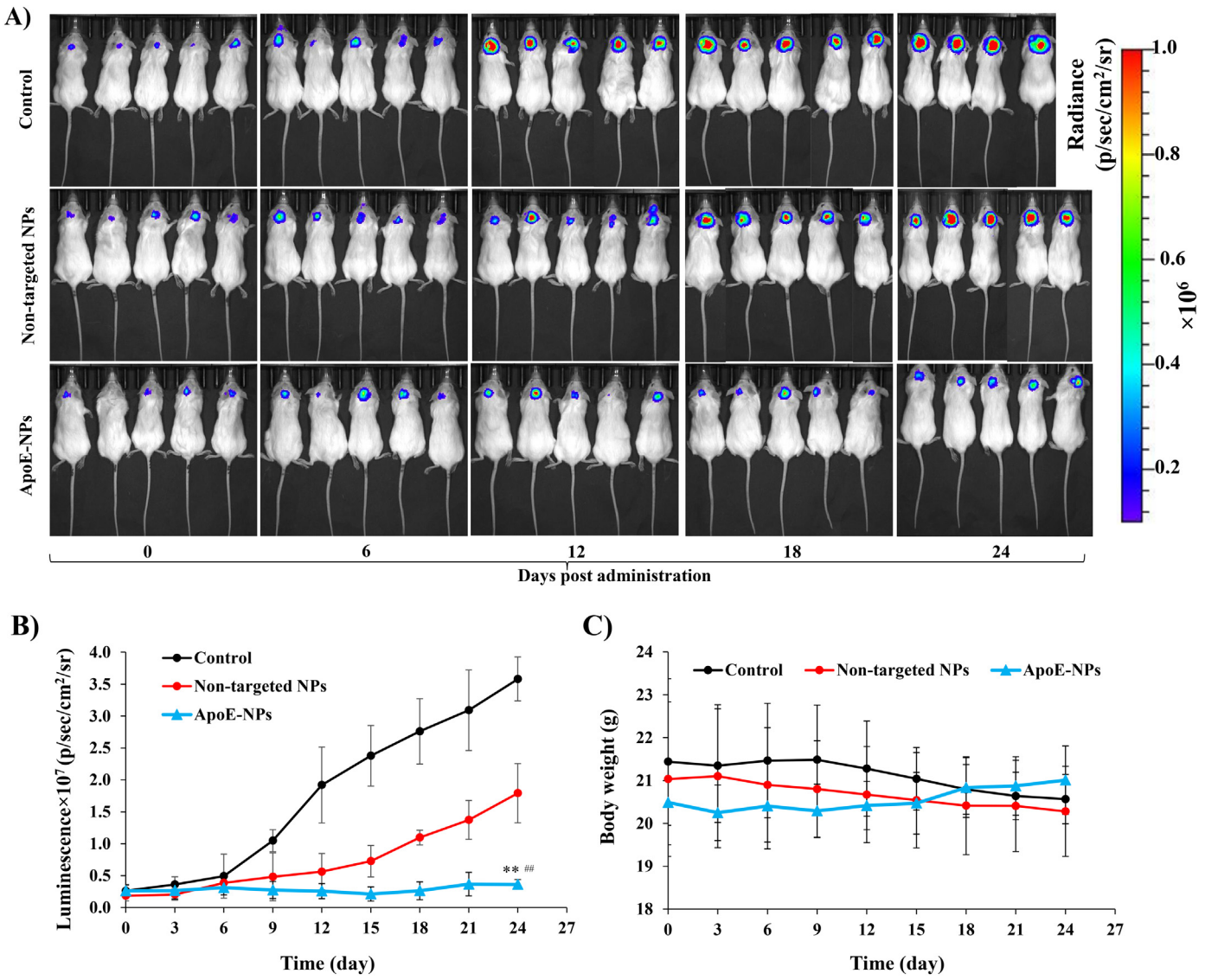

Fig. 9. In vivo therapeutic effects of orthotopic MB bearing mice after systemic administration of ApoE targeted and non-targeted JQ1 loaded nanoparticles (NPs) at the dose of 10 mg/kg every 3 days. (A) Bioluminescence image at different times; (B) Quantitative analysis of IVIS signal intensity (photons/s/cm^2/sr) over time after injection; (C) Mouse body weight changes during treatment.

target the liposomes to the brain in vitro and in vivo, we speculate this may be due to the low density of target ligand on the liposome surface [39,40]. It has been shown previously that the targeting efficiency of NPs or liposomes was significantly affected by the density of targeting ligand. In our research, NPs were prepared using 30% of COG-133 conjugated PEG-PBC polymer and 70% of mPEG-PCD polymer which could increase the binding efficiency of our NPs to LDLR, leading to the higher JQ1 accumulation in the brain (Fig. 7).

To demonstrate that ApoE-NPs could improve anticancer efficiency in vivo, orthotopic MB bearing mice was established via stereotaxic injections of stably luciferase expressing HD-MB03 cells into cerebellum. Luciferase signals of tumor cells were significantly decreased after treatment with JQ1 loaded ApoE-NPs compared to the control and non-targeted NPs groups (Fig. 9), suggesting ApoE mimetic peptide conjugated JQ1 loaded NPs have the potential to enhance drug delivery to the brain and enhance its therapeutic efficacy. Moreover, treatment with ApoE-NPs remarkably inhibited MB cell proliferation and induced cell apoptosis compared to non-targeted NPs caused by targeted accumulation which consistent with cell cycle arrest and apoptosis induction in vitro.

5. Conclusion

In conclusion, COG-133 conjugated PEG-PBC has the potential to efficiently encapsulate JQ1 and other hydrophobic drugs into NPs. In this study, systemic administration of JQ1 loaded ApoE-NPs significantly inhibited MB progression in orthotopic mouse model compared to the control and JQ1 loaded non-targeted NPs.

Contributions

Q.W., V.K., D.W.C., T.M. and R.I.M. conceived and designed the project. Q.W., F.L. and B.S. conducted the experiments. Q.W., V.K. and R.I.M. analyzed the data and prepared the manuscript. All authors read and approved the manuscript.

Declaration of Competing Interest

The authors declare no conflict of interest.

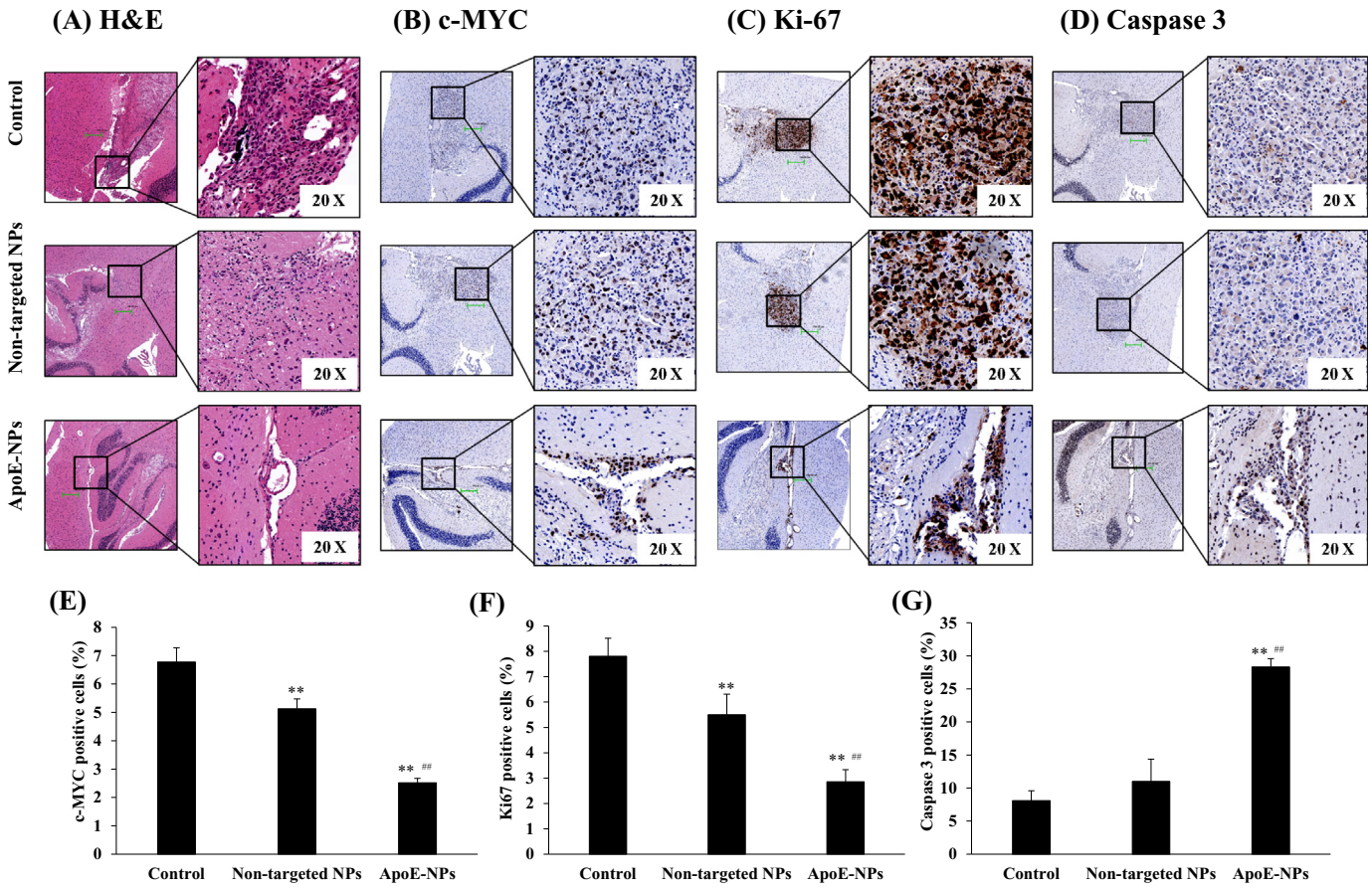

Fig. 10. Effect of JQ1 treatment on tumor growth and tumor cell apoptosis. Medulloblastoma from control, JQ1 loaded non-targeted NPs and JQ1 loaded ApoE-NPs treated groups were stained by A) hematoxylin and eosin (H&E), B) c-MYC, C) Ki-67, and D) cleaved Caspase 3. The percentage of E) c-MYC positive cells; F) Ki67 positive cells; G) Caspase 3 positive cells. **, $p < .01$ (comparison between ApoE-NPs vs Control), ##, $p < .01$ (comparison between ApoE-NPs vs Non-targeted NPs).

Acknowledgments

We greatly acknowledge the financial support of the Pediatric Cancer Research Group of the University of Nebraska Medical Center and Children's Hospital (LB805) and The Team Jack Foundation for this work.

Appendix A. Supplementary data

Supplementary data to this article can be found online at https://doi.org/10.1016/j.jconrel.2020.04.053.

References

[1] V. Kumar, V. Kumar, T. McGuire, D.W. Coulter, J.G. Sharp, R.I. Mahato, Challenges and recent advances in Medulloblastoma therapy, Trends Pharmacol. Sci. 38 (2017) 1061–1084 (DOI:S0165-6147(17)30181-5 [pii]).

[2] R.J. Packer, A. Gajjar, G. Vezina, L. Rorke-Adams, P.C. Burger, P.L. Robertson, L. Bayer, D. LaFond, B.R. Donahue, M.H. Marymont, K. Muraszko, J. Langston, R. Sposto, Phase III study of craniospinal radiation therapy followed by adjuvant chemotherapy for newly diagnosed average-risk medulloblastoma, J. Clin. Oncol. 24 (2006) 4202–4208 (DOI:24/25/4202 pii).

[3] P.R. Thomas, M. Deutsch, J.L. Kepner, J.M. Boyett, J. Krischer, P. Aronin, L. Albright, J.C. Allen, R.J. Packer, R. Linggood, R. Mulhern, J.A. Stehbens, J. Langston, P. Stanley, P. Duffner, L. Rorke, J. Cherlow, H.S. Friedman, J.L. Finlay, T.J. Vietti, L.E. Kun, Low-stage medulloblastoma: final analysis of trial comparing standard-dose with reduced-dose neuraxis irradiation, J. Clin. Oncol. 18 (2000) 3004–3011, https://doi.org/10.1200/JCO.2000.18.16.3004.

[4] M.C. Cox, J.M. Kusters, C.E. Gidding, J.H. Schieving, E.J. van Lindert, J.H. Kaanders, G.O. Janssens, Acute toxicity profile of craniospinal irradiation with intensity-modulated radiation therapy in children with medulloblastoma: A prospective analysis, Radiat. Oncol. 10 (2015), https://doi.org/10.1186/s13014-015-0547-9 241–015.

[5] Anonymous medulloblastoma, Nat. Rev. Dis. Primers 5 (2019), https://doi.org/10.1038/s41572-019-0067-2 12–019.

[6] Y. Tang, S. Gholamin, S. Schubert, M.I. Willardson, A. Lee, P. Bandopadhayay, G. Bergthold, S. Masoud, B. Nguyen, N. Vue, B. Balansay, F. Yu, S. Oh, P. Woo, S. Chen, A. Ponnuswami, M. Monje, S.X. Atwood, R.J. Whitson, S. Mitra, S.H. Cheshier, J. Qi, R. Beroukhim, J.Y. Tang, R. Wechsler-Reya, A.E. Oro, B.A. Link, J.E. Bradner, Y.J. Cho, Epigenetic targeting of Hedgehog pathway transcriptional output through BET bromodomain inhibition, Nat. Med. 20 (2014) 732–740, https://doi.org/10.1038/nm.3613.

[7] G. Barone, J. Anderson, A.D. Pearson, K. Petrie, L. Chesler, New strategies in neuroblastoma: therapeutic targeting of MYCN and ALK, Clin. Cancer Res. 19 (2013) 5814–5821, https://doi.org/10.1158/1078-0432.CCR-13-0680.

[8] N. Wen, B. Guo, H. Zheng, L. Xu, H. Liang, Q. Wang, D. Wang, X. Chen, S. Zhang, Y. Li, L. Zhang, Bromodomain inhibitor jq1 induces cell cycle arrest and apoptosis of glioma stem cells through the VEGF/PI3K/AKT signaling pathway, Int. J. Oncol. 55 (2019) 879–895, https://doi.org/10.3892/ijo.2019.4863.

[9] S. Hutter, S. Bolin, H. Weishaupt, F.J. Swartling, Modeling and targeting MYC genes in childhood brain tumors, Genes (Basel) (2017) 8, https://doi.org/10.3390/genes8040107 (DOI:E107 [pii]).

[10] Y. Li, Q. Song, B.W. Day, Phase I and phase II sonidegib and vismodegib clinical trials for the treatment of paediatric and adult MB patients: a systemic review and meta-analysis, Acta Neuropathol. Commun. 7 (2019), https://doi.org/10.1186/s40478-019-0773-8 123–019.

[11] S. Buonamici, J. Williams, M. Morrissey, A. Wang, R. Guo, A. Vattay, K. Hsiao, J. Yuan, J. Green, B. Ospina, Q. Yu, L. Ostrom, P. Fordjour, D.L. Anderson, J.E. Monahan, J.F. Kelleher, S. Peukert, S. Pan, X. Wu, S.M. Maira, C. Garcia-Echeverria, K.J. Briggs, D.N. Watkins, Y.M. Yao, C. Lengauer, M. Warmuth, W.R. Sellers, M. Dorsch, Interfering with resistance to smoothened antagonists by inhibition of the PI3K pathway in medulloblastoma, Sci. Transl. Med. 2 (2010) 51ra70, https://doi.org/10.1126/scitranslmed.3001599.

[12] G.J. Dijkgraaf, B. Alicke, L. Weinmann, T. Januario, K. West, Z. Modrusan, D. Burdick, R. Goldsmith, K. Robarge, D. Sutherlin, S.J. Scales, S.E. Gould, R.L. Yauch, F.J. de Sauvage, Small molecule inhibition of GDC-0449 refractory smoothened mutants and downstream mechanisms of drug resistance, Cancer Res. 71 (2011) 435–444, https://doi.org/10.1158/0008-5472.CAN-10-2876.

[13] P. Filippakopoulos, J. Qi, S. Picaud, Y. Shen, W.B. Smith, O. Fedorov, E.M. Morse, T. Keates, T.T. Hickman, I. Felletar, M. Philpott, S. Munro, M.R. McKeown, Y. Wang, A.L. Christie, N. West, M.J. Cameron, B. Schwartz, T.D. Heightman, N. La Thangue, C.A. French, O. Wiest, A.L. Kung, S. Knapp, J.E. Bradner, Selective inhibition of BET bromodomains, Nature 468 (2010) 1067–1073, https://doi.org/10.1038/nature09504.

[14] A. Puissant, S.M. Frumm, G. Alexe, C.F. Bassil, J. Qi, Y.H. Chanthery, E.A. Nekritz, R. Zeid, W.C. Gustafson, P. Greninger, M.J. Garnett, U. McDermott, C.H. Benes, A.L. Kung, W.A. Weiss, J.E. Bradner, K. Stegmaier, Targeting MYCN in neuroblastoma by BET bromodomain inhibition, Cancer. Discov. 3 (2013) 308–323, https://doi.org/10.1158/2159-8290.CD-12-0418.

[15] H. Maeda, Polymer therapeutics and the EPR effect, J. Drug Target. 25 (2017) 781–785, https://doi.org/10.1080/1061186X.2017.1365878.

[16] M. Danquah, T. Fujiwara, R.I. Mahato, Self-assembling methoxypoly(ethylene glycol)-b-poly(carbonate-co-L-lactide) block copolymers for drug delivery, Biomaterials 31 (2010) 2358–2370, https://doi.org/10.1016/j.biomaterials.2009.11.081.

[17] D. Chitkara, S. Singh, V. Kumar, M. Danquah, S.W. Behrman, N. Kumar, R.I. Mahato, Micellar delivery of cyclopamine and gefitinib for treating pancreatic cancer, Mol. Pharm. 9 (2012) 2350–2357, https://doi.org/10.1021/mp3002792.

[18] D. Chitkara, A. Mittal, S.W. Behrman, N. Kumar, R.I. Mahato, Self-assembling, amphiphilic polymer-gemcitabine conjugate shows enhanced antitumor efficacy against human pancreatic adenocarcinoma, Bioconjug. Chem. 24 (2013) 1161–1173, https://doi.org/10.1021/bc400032x.

[19] C. Qiao, J. Yang, Q. Shen, R. Liu, Y. Li, Y. Shi, J. Chen, Y. Shen, Z. Xiao, J. Weng, X. Zhang, Traceable nanoparticles with dual targeting and ROS response for RNAi-based immunochemotherapy of intracranial glioblastoma treatment, Adv. Mater. 30 (2018), https://doi.org/10.1002/adma.201705054 e1705054.

[20] Y. Zhu, Y. Jiang, F. Meng, C. Deng, R. Cheng, J. Zhang, J. Feijen, Z. Zhong, Highly efficacious and specific anti-glioma chemotherapy by tandem nanomicelles co-functionalized with brain tumor-targeting and cell-penetrating peptides, J. Control. Release 278 (2018) 1–8 (DOI:S0168-3659(18)30155-X [pii]).

[21] F. Li, M. Danquah, R.I. Mahato, Synthesis and characterization of amphiphilic lipopolymers for micellar drug delivery, Biomacromolecules 11 (2010) 2610–2620, https://doi.org/10.1021/bm100561v.

[22] N. Balaji, M. Chinnapattu, A. Dixit, P. Sahu, S.S. P, R. Mullangi, Validation of an enantioselective LC-MS/MS method to quantify enantiomers of (+/−)-OTX015 in mice plasma: Lack of in vivo inversion of (−)-OTX015 to its antipode, Biomed. Chromatogr. 31 (2017), https://doi.org/10.1002/bmc.3853 Epub 2016 Oct 14.

[23] A.M. Martin, E. Raabe, C. Eberhart, K.J. Cohen, Management of pediatric and adult patients with medulloblastoma, Curr. Treat. Options in Oncol. 15 (2014) 581–594, https://doi.org/10.1007/s11864-014-0306-4.

[24] P.M. Zeltzer, J.M. Boyett, J.L. Finlay, A.L. Albright, L.B. Rorke, J.M. Milstein, J.C. Allen, K.R. Stevens, P. Stanley, H. Li, J.H. Wisoff, J.R. Geyer, P. McGuire-Cullen, J.A. Stehbens, S.B. Shurin, R.J. Packer, Metastasis stage, adjuvant treatment, and residual tumor are prognostic factors for medulloblastoma in children: conclusions from the Children's Cancer Group 921 randomized phase III study, J. Clin. Oncol. 17 (1999) 832–845, https://doi.org/10.1200/JCO.1999.17.3.832.

[25] J. Wang, A. Garancher, V. Ramaswamy, R.J. Wechsler-Reya, Medulloblastoma: From Molecular Subgroups to Molecular Targeted Therapies, Annu. Rev. Neurosci. 41 (2018) 207–232, https://doi.org/10.1146/annurev-neuro-070815-013838.

[26] A. Henssen, T. Thor, A. Odersky, L. Heukamp, N. El-Hindy, A. Beckers, F. Speleman, K. Althoff, S. Schafers, A. Schramm, U. Sure, G. Fleischhack, A. Eggert, J.H. Schulte, BET bromodomain protein inhibition is a therapeutic option for medulloblastoma, Oncotarget 4 (2013) 2080–2095 (DOI:1534 [pii]).

[27] P. Mill, R. Mo, M.C. Hu, L. Dagnino, N.D. Rosenblum, C.C. Hui, Shh controls epithelial proliferation via independent pathways that converge on N-Myc, Dev. Cell 9 (2005) 293–303 (DOI:S1534-5807(05)00179-6 [pii]).

[28] S. Venkataraman, I. Alimova, I. Balakrishnan, P. Harris, D.K. Birks, A. Griesinger, V. Amani, B. Cristiano, M. Remke, M.D. Taylor, M. Handler, N.K. Foreman, R. Vibhakar, Inhibition of BRD4 attenuates tumor cell self-renewal and suppresses stem cell signaling in MYC driven medulloblastoma, Oncotarget 5 (2014) 2355–2371 (DOI:1659 [pii]).

[29] F.H. Andrews, A.R. Singh, S. Joshi, C.A. Smith, G.A. Morales, J.R. Garlich, D.L. Durden, T.G. Kutateladze, Dual-activity PI3K-BRD4 inhibitor for the orthogonal inhibition of MYC to block tumor growth and metastasis, Proc. Natl. Acad. Sci. U. S. A. 114 (2017) E1072–E1080, https://doi.org/10.1073/pnas.1613091114.

[30] X. Zhu, K. Enomoto, L. Zhao, Y.J. Zhu, M.C. Willingham, P. Meltzer, J. Qi, S.Y. Cheng, Bromodomain and extraterminal protein inhibitor JQ1 suppresses thyroid tumor growth in a mouse model, Clin. Cancer Res. 23 (2017) 430–440, https://doi.org/10.1158/1078-0432.CCR-16-0914.

[31] M.K. Mateyak, A.J. Obaya, J.M. Sedivy, c-Myc regulates cyclin D-Cdk4 and -Cdk6 activity but affects cell cycle progression at multiple independent points, Mol. Cell. Biol. 19 (1999) 4672–4683, https://doi.org/10.1128/mcb.19.7.4672.

[32] Y. Qi, Y. Tu, D. Yang, Q. Chen, J. Xiao, Y. Chen, J. Fu, X. Xiao, Z. Zhou, Cyclin A but not cyclin D1 is essential for c-myc-modulated cell-cycle progression, J. Cell. Physiol. 210 (2007) 63–71, https://doi.org/10.1002/jcp.20816.

[33] W.M. Pardridge, The blood-brain barrier: bottleneck in brain drug development, NeuroRx 2 (2005) 3–14, https://doi.org/10.1602/neurorx.2.1.3.

[34] A.R. Jones, E.V. Shusta, Blood-brain barrier transport of therapeutics via receptor-mediation, Pharm. Res. 24 (2007) 1759–1771, https://doi.org/10.1007/s11095-007-9379-0.

[35] J.M. Lajoie, E.V. Shusta, Targeting receptor-mediated transport for delivery of biologics across the blood-brain barrier, Annu. Rev. Pharmacol. Toxicol. 55 (2015) 613–631, https://doi.org/10.1146/annurev-pharmtox-010814-124852.

[36] J. Paterson, C.I. Webster, Exploiting transferrin receptor for delivering drugs across the blood-brain barrier, Drug Discov. Today Technol. 20 (2016) 49–52 (DOI:S1740-6749(16)30023-3 [pii]).

[37] R. Dal Magro, F. Ornaghi, I. Cambianica, S. Beretta, F. Re, C. Musicanti, R. Rigolio, E. Donzelli, A. Canta, E. Ballarini, G. Cavaletti, P. Gasco, G. Sancini, ApoE-modified solid lipid nanoparticles: a feasible strategy to cross the blood-brain barrier, J. Control. Release 249 (2017) 103–110 (DOI:S0168-3659(16)31113-0 [pii]).

[38] A.R. Neves, J.F. Queiroz, S. Reis, Brain-targeted delivery of resveratrol using solid lipid nanoparticles functionalized with apolipoprotein E, J. Nanobiotechnol. 14 (2016), https://doi.org/10.1186/s12951-016-0177-x 27–016.

[39] I. van Rooy, E. Mastrobattista, G. Storm, W.E. Hennink, R.M. Schiffelers, Comparison of five different targeting ligands to enhance accumulation of liposomes into the brain, J. Control. Release 150 (2011) 30–36, https://doi.org/10.1016/j.jconrel.2010.11.014.

[40] I. van Rooy, W.E. Hennink, G. Storm, R.M. Schiffelers, E. Mastrobattista, Attaching the phage display-selected GLA peptide to liposomes: factors influencing target binding, Eur. J. Pharm. Sci. 45 (2012) 330–335, https://doi.org/10.1016/j.ejps.2011.11.015.